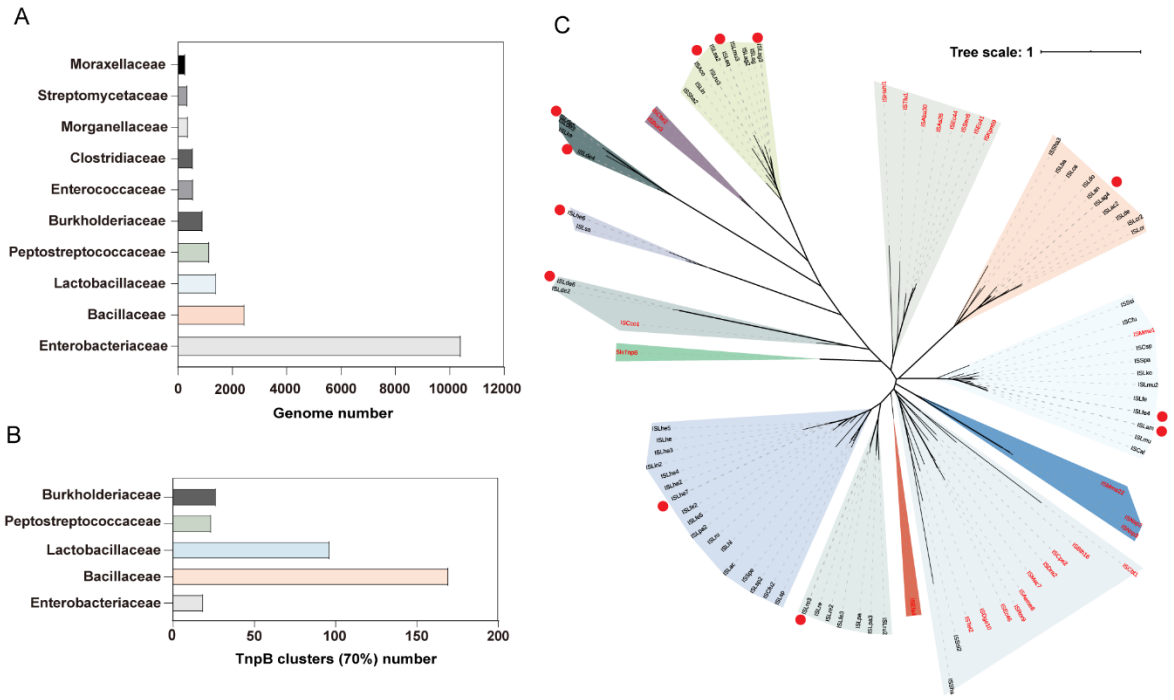

Supplementary Figure 1. Genomic distribution, diversity, and phylogenetic relationships of TnpB endonuclease. A, Quantitative distribution of genomes containing multicopy TnpB across taxonomic families in the NCBI database. **B,** Diversity of TnpB systems clustered at a 70% similarity threshold across taxonomic families. **C,** Phylogenetic relationships of 64 *Lactobacillus*-derived TnpB systems with previously reported active TnpB systems. Red circles, candidates selected in this study; red font, previously reported active TnpBs.

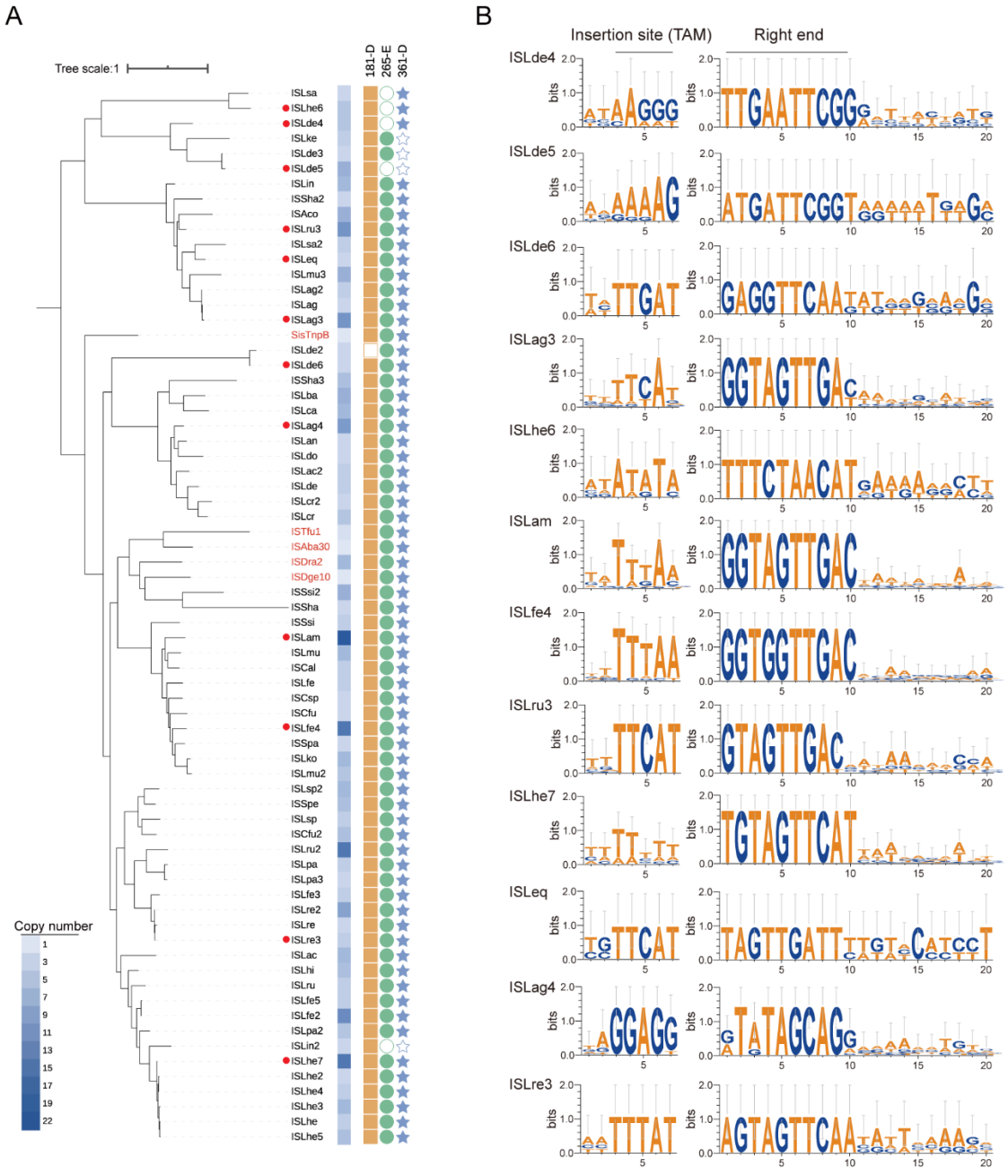

Supplementary Figure 2. Phylogenetic analysis of 65 Lactobacillaceae-derived TnpB systems and identification of TAM and ωRNA. A, Phylogenetic distribution of 65 unique Lactobacillaceae-derived TnpB endonuclease together with SisTnpB1, ISTfu1, ISAba30, ISDra2, and ISDge10 TnpB endonuclease. Blue squares, the copy number of each TnpB system. All TnpB amino acid sequences were aligned to ISDra2

to assess the key residues in the RuvC domain. Orange squares, D181; green circles, E256; blue pentagrams, D361. **B,** Left ends and right ends of 12 Lactobacillaceae-derived TnpB systems identified using WebLogo analysis. The left ends used to identify putative TAMs and the right ends used to identify putative ωRNAs.

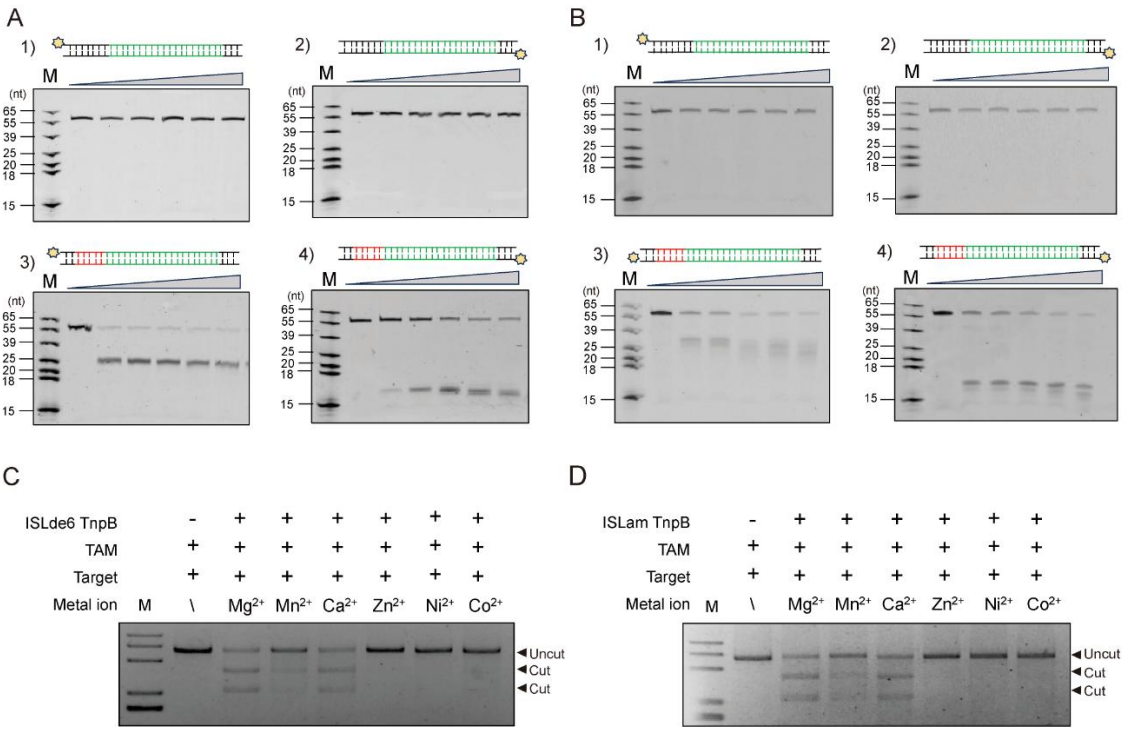

Supplementary Figure 3. ***In vitro*** **DNA cleavage by TnpB RNP complex. A** and **B,** Cleavage of Synthetic dsDNA substartes with or without a TAM (red) sequence by ISLde6 (**A**) and ISLam (**B**) TnpB RNP complexes. NTS and TS indicate non-target and target strands, respectively. M, DNA marker. Reaction samples were collected at 0 min, 1 min, 5 min, 15 min, 30 min, and 1 h, with "0" representing substrate only. **C** and **D,** Metal ion–dependent endonuclease activity of ISLde6 (**C**) and ISLam (**D**) TnpB RNP complexes at 37°C.

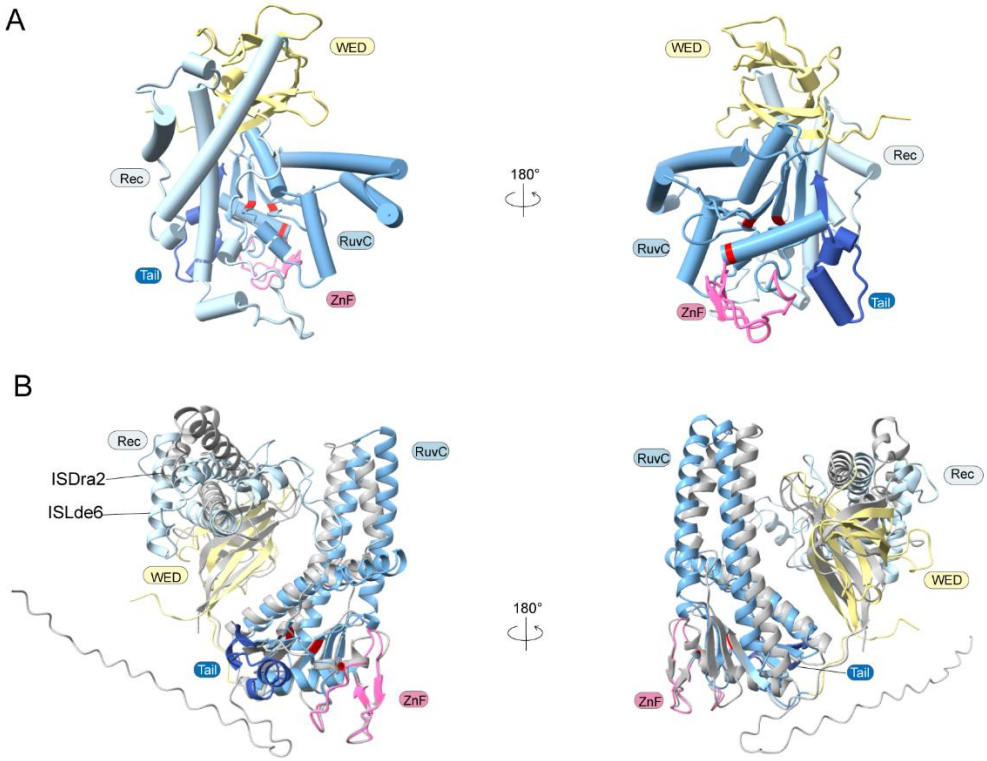

Supplementary Figure 4. Structure prediction of ISLde6 TnpB and comparison with ISDra2 TnpB. A, Predicted structure of ISLde6 TnpB by AlphaFold3. **B,** Structural superposition of the predicted ISLde6 TnpB model onto the ISDra2 TnpB structure. The ISDra2 TnpB structure is shown in gray, and the ISLde6 TnpB model is shown in color.

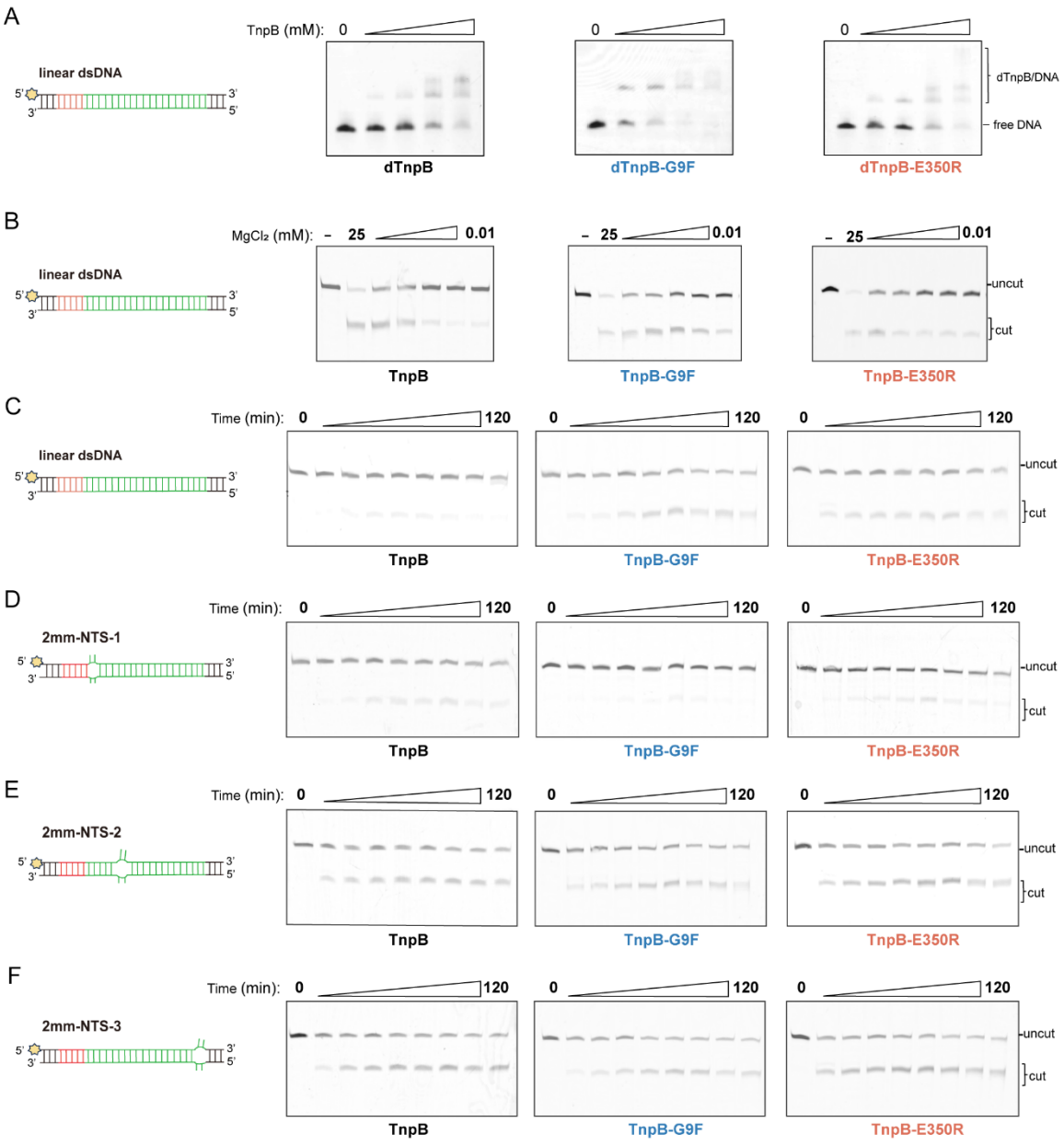

Supplementary Figure 5. ***In vitro*** **EMSA and cleavage assays of TnpB and its variants, related to Figure 5.** All cleavage assays were performed using denaturing PAGE. Reaction time points were collected at 0, 0.5, 1, 2, 5, 10, 30, 60, and 120 minutes for kinetic analyses. **A,** EMSA analysis of 5′-FAM–labeled dsDNA (2 nM) with dTnpB, dTnpB-G9F, dTnpB-E350R RNP complex (50, 100, 150 and 200nM) under 10mM Mg^{2+}. **B,** *In vitro* cleavage of 59-nt dsDNA by TnpB, TnpB-G9F and TnpB-E350R for

60min across a range of Mg^{2+} concentrations (25, 2.5, 0.25, 0.1, 0.025, and 0.01 mM), related to Figure 5c. **C,** *In vitro* cleavage of a 59-nt dsDNA substrate by TnpB, TnpB-G9F and TnpB-E350R under 0.1 mM Mg^{2+}. **D-F,** *In vitro* cleavage of pre-unwound substrate 2mm-NTS-1, 2mm-NTS-2 and 2mm-NTS-3 by TnpB, TnpB-G9F and TnpB-E350R under 0.1 mM Mg^{2+}, respectively. The pre-unwound substrates 2mm-NTS-1, 2mm-NTS-2, and 2mm-NTS-3 were derived from the linearized dsDNA substrate by introducing two mismatched nucleotides within the NTS strand at positions 1–2, 6–7, and 19–20, respectively, mimicking pre-unwound DNA structures.

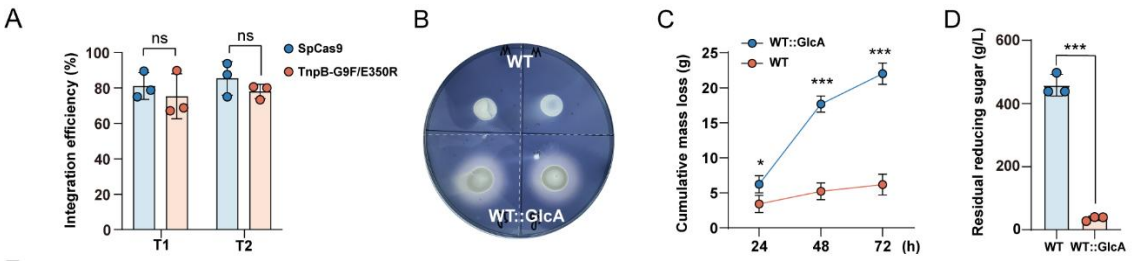

Supplementary Figure 6. FIRE-TnpB mediates efficient integration of both small and large biosynthetic pathways in industrial diploid *S. cerevisiae* M. A, Integration efficiency of a 2.8-kb glucoamylase expression cassette (GlcA) at two genomic loci in the diploid industrial *S. cerevisiae* strain M by TnpB-G9F/E350R compared with SpCas9. **B,** Iodine staining of starch agar plates to assess glucoamylase activity. Clear halos surrounding colonies (WT::GlcA) indicate starch hydrolysis. **C,** Fermentation profiles showing cumulative mass loss curves (CO_2 release) during ethanol production from starch by the wild-type and GlcA-integrated.